ROYAL SOCIETY OF CHEMISTRY

PAPER

Check for updates

Performance of the highly sensitive humidity sensor constructed with nanofibrillated cellulose/graphene oxide/polydimethylsiloxane aerogel *via* freeze drying

Yutong Yang, Guoting Su, Qilin Li, Zipiao Zhu, Shaoran Liu, Bing Zhuo, Xinpu Li, Pu Ti and Quanping Yuan [ID] *

A kind of capacitive humidity sensor with high sensitivity constructed with nanofibrillated cellulose (NFC), graphene oxide (GO) and polydimethylsiloxane (PDMS) is presented in this work, *via* a simple ultrasonic dispersion and freeze drying technology. The NFC and GO with a strong adsorption for water molecules were used as a substrate for the promotion of capacitive response of the humidity sensor. Moreover, anhydrous ethanol was added to inhibit the generation of big cracks in the humidity sensor in the freeze drying process, so as to obtain a regular network porous structure, then providing a great deal of conduction channels and active sites for molecular water. Also, the addition of PDMS can effectively enhance the flexibility and stability of its porous structure. The results confirmed that the humidity sensor with 30 wt% GO showed an excellent humidity sensitivity (6576.41 pF/% RH), remarkable reproducibility, low humidity hysteresis characteristic in 11–97% relative humidity (RH) at 25 °C, and short response/recovery times (57 s/2 s). In addition, the presented sensor exhibited small relative deviation of the measured relative humidity value compared with the commercial hygrometer. The realization of the high sensitivity can be attributed to the theories about interaction of the hydrophilic group, proton transfer of water molecules and the three-dimensional network transport structure model. Therefore, the NFC/GO/PDMS humidity sensor finally realizes stable, reproducible and fast humidity sensing *via* an eco-friendly process, exhibiting promising potential for wide practical application.

Introduction

With the development of an intelligent modern society, humidity sensors are widely used in multifarious fields such as environmental monitoring,[1] automobile defogging,[2] production line,[3] respiratory monitoring,[4-6] medical care,[7] agriculture and forestry breeding,[8] meteorological detection,[9] food logistics and transportation,[10] and wearable flexible equipment.[11] As a precision instrument for humidity measurement, it is highly vital for a humidity sensor to satisfy higher requirements for its accuracy, sensitivity, excellent stability and compatibility. However, for traditional humidity sensors there exist some challenges such as low sensitivity, lag response and insufficient sensing efficiency.[12] Therefore, the development of flexible, efficient and green humidity sensitive materials becomes the theme for the future development of humidity sensors.

Humidity sensors can detect humidity *via* sensing the change of electrical signal induced by the absorption or desorption of water molecules in the tested environment. Up to

School of Resources, Environment and Materials, Guangxi University, Nanning 530004, China. E-mail: yuanquanping@gxu.edu.cn

now, a variety of metal oxides,[13] organic polymers,[14] and carbon materials[15] were used to prepare resistance type,[16] capacitance type,[8] optical fiber type,[17] quartz crystal microbalance type[3] and other types of humidity sensors. Graphene oxide (GO), nano-fibrillated cellulose (NFC) and polydimethylsiloxane (PDMS) are extensively introduced in humidity sensing due to their unique properties. As a multifunctional derivative of graphene, GO is rich in hydrophilic groups (such as hydroxyl (–OH) and carboxyl (–COOH)), and has a large specific surface area. It has a high degree of participation in the construction of two-dimensional or three-dimensional network structure, which can provide a large number of active sites to absorb water molecules, greatly improving its humidity sensing characteristics and becoming a potential sensor material.[18-20] In recent years, there were many reports related to the development of GO-based humidity sensor. For example, Xuan *et al.* prepared flexible humidity sensor with GO sensing layer that possessed high sensitivity and response speed *via* dropping casting.[21] Another humidity sensitive polymer material made of GO, Nafion and In₂O₃, also presents high sensitivity, good stability and rapid response (70 s).[22] To further improve response speed of humidity sensor, Zhang *et al.* proposed to develop a super sensitive GO/SnS₂

humidity sensor on a flexible substrate,[23] obtaining outstanding response (0.9 s) and recovery (10 s) performance, as well as excellent reproducibility.[23]

As a renewable and natural biomass polymer, nanocellulose has the advantages of biodegradability, excellent mechanical strength, large specific surface area, and self-assemble performance. It is also a good surfactant, which can enhance the dispersion and compatibility of carbon materials.[4] Due to the hydrophilic groups such as –OH and –COOH on cellulose molecules,[24] cellulose are more sensitive to temperature and humidity. A polymer film compounded by NFC, reduced graphene oxide (rGO) and polyvinyl alcohol (PVA), exhibited better humidity sensing performance compared to PVA/rGO film without NFC.[25] Thus, the characteristics of nanocellulose make it have great potential in sensor applications, especially in humidity sensing.[26–28] Besides, Yao *et al.* developed another nanocellulose based quartz crystal microbalance (QCM) humidity sensor with asymmetric structure, presenting the characteristics of short response/recovery time (60 s/15 s), low humidity hysteresis (7.3% RH), and excellent long-term stability.[29] Combining polypyrrole and nanocellulose is to obtain humidity sensor with good humidity sensitivity, remarkable linearity and superior reversibility.[30] A large number of studies had proved that specific surface area and number of hydrophilic groups of the sensing material have a great impact on its sensitivity, response speed, humidity hysteresis performance and long-term stability.[29] Therefore, the development of highly sensitive, highly stable and environment-friendly humidity sensor with nanocellulose has a great prospect.

However, a single sensing material still has certain defects in the response performance of the sensor in the high relative humidity range.[31] Our work proposed to use ultrasonic dispersion and vacuum freeze drying method to install NFC/GO/PDMS aerogel with abundant three-dimensional porous structure on the flexible interdigital electrode to prepare a new kind of NFC/GO/PDMS humidity sensor. The use of NFC and GO with numbers of hydrophilic groups attracting more water molecules can increase the response of sensor.[32] Moreover, previous researches had pointed out that the enhancement of interfacial interaction can change the dielectric properties of composite materials.[32,33] So the interaction among NFC, GO and PDMS will lead to changes in its dielectric properties and the promotion of capacitive response. Especially, a certain amount of anhydrous ethanol was added into the dispersion system of NFC and GO, by which the cracks in NFC/GO/PDMS can be reduced in the freeze drying process.[34] The imposed small amount of PDMS had also enhanced connects among NFC and GO, by which the three-dimensional porous network structure became more stable and the adhesion of the aerogel on the electrode was further strengthened, so as to obtain remarkable reproducibility. Hence, the presented method will further elevate the performance of the capacitance humidity sensor for wide and practical application.

Experimental

Material

The GO dispersion (2 mg mL^{-1}) was obtained from Suzhou Tanfeng Graphene Technology Co., Ltd. (Suzhou, China). The NFC dispersion (1.08 wt%) was supplied by Tianjin Woodelf Biotechnology Co., Ltd. (Tianjin, China). Anhydrous ethanol was purchased from Chengdu Chron Chemicals Co., Ltd. (AR; Chengdu, China). Polydimethylsiloxanes (Sylgard184, PDMS) were prepared by Dow Corning Co., Ltd. Flexible interdigital electrode (IDE; width, length, thickness: 5 mm × 10 mm × 0.1 mm), is made of polyethylene terephthalate (PET) substrate plated with metal copper/nickel/gold, and the interdigital gap and width are 100 μm, as well as the effective area is 25 mm^2.

Preparation of NFC/GO/PDMS aerogel and humidity sensor

The NFC/GO/PDMS aerogel and humidity sensor were prepared *via* follow process. First, after weighting 24 mg NFC in a beaker, 1.7 mL anhydrous ethanol and 1.7 mL deionized water were added in that to mix sufficiently. Then the mixture was treated using an ultrasonic cell breaker (TL-1200Y, Jiangsu Tenlin Instrument Co., Ltd., Yancheng, China) for 10 min under the power of 1000 W. Follow by 6 mL GO dispersion (GO content of 30 wt%) was blended into the above mixture with ultrasound treatment for 50 min under the power of 1000 W. After that,
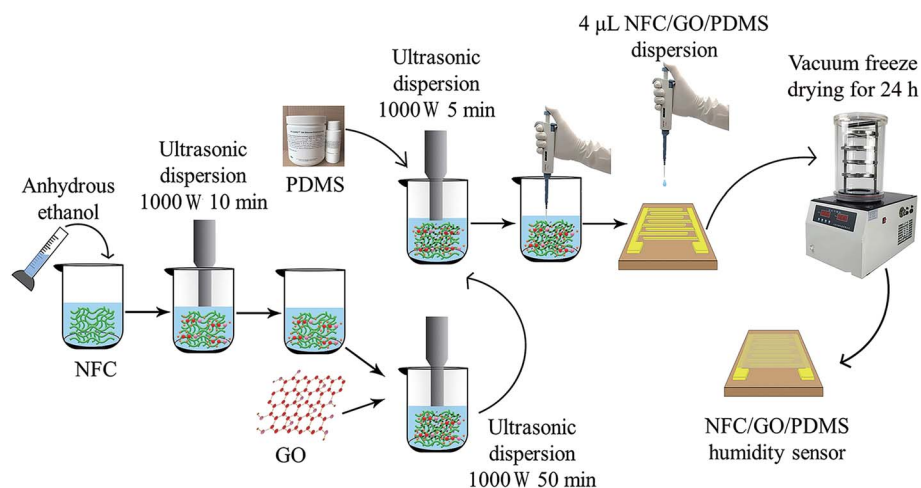

Fig. 1 Fabrication process of the humidity sensor.

4 mg PDMS was uniformly mingled with the mixture. Sequentially, the mixture dispersion was disposed for 5 min *via* ultrasonication under 1000 W. Hereto, NFC/GO/PDMS composite dispersion with a certain mass ratio was obtained.

The 4 μL composite dispersion was dropped on the flexible interdigital electrode through a micro pipette, and then was spread over its effective interdigital area. Successively, the treated interdigital electrode was put into the vacuum freeze dryer (Fd-1A-50, Jiangsu Tenlin Instrument Co., Ltd., Yancheng, China) to freeze for 3 h and then vacuum dry for 24 h. Finally, the prepared humidity sensor was gained. The specific process is shown in Fig. 1. The humidity sensors with different GO contents (10 wt%, 20 wt%, 30 wt%, and 40 wt%) were fabricated by referring to the above method. In which, the NFC/GO/PDMS composite dispersion had the controlled concentration of 3.5 mg mL^{-1} (the content of NFC changed with the content of GO, and the addition amount of PDMS was controlled at 10 wt%). Their humidity sensing performance and mechanism were studied.

Meanwhile, the above remaining composite dispersion after sucked to prepare sensor, was put into a Petri dish (disk shape, 55 mm in diameter) and a small beaker (cylinder shape; 22 mm × 22 mm × 25 mm), respectively. The two shape of the aerogel were formed after dried using the same vacuum freeze drying process. The obtained NFC/GO/PDMS aerogel were taken to investigate their surface morphology, density, flexibility and chemical properties.

Humidity sensing measurement

The humidity sensing performance was tested by exposing the prepared sensor in measurement space with various relative humidity which are provided by using saturated salt solution of LiCl (11% RH), MgCl$_2$ (33% RH), NaBr (58% RH), NaCl (75% RH), KCl (85% RH) and K$_2$SO$_4$ (97% RH) under the room temperature of 25 °C. The output capacitance value of the sensor was measured through LCR digital bridge (4091 C; Double King Industrial Holdings Co., Ltd., Shenzhen, China) under the certain temperature and different humidity conditions at the frequency of 100 Hz. The test device is shown in Fig. 2. A commercial hygrometer (AS847, ±3% RH; ARCO Electronics Co., Ltd., Guangzhou, China) was also applied to test the humidity of environment for reducing the test error. Sensitivity, response/recovery time and humidity hysteresis are important indexes to evaluate performance of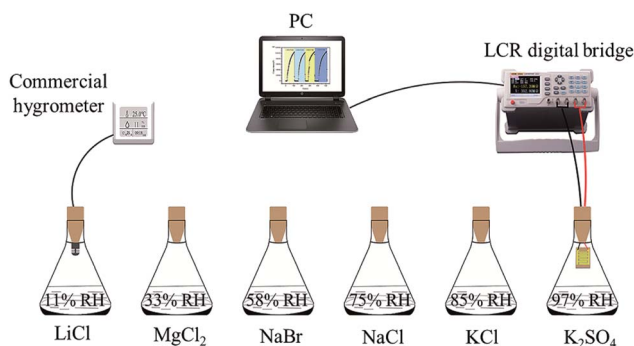 the sensor. Here, the ratio of capacitance difference and humidity difference under a certain humidity condition is defined as the sensitivity (S), $S = (C_x - C_0)/(RH_{97} - RH_{11})$. The response time is defined as the required time when capacitance change of the sensor reaches 90% of the value of $|C_x - C_0|$. And the recovery time refers to the time from the response equilibrium state back to initial state. Specifically, the capacitance value of the sensor at 11% RH was defined as the initial capacitance C_0, and C_x represent the capacitance value at 97% RH.

The reproducibility of the sensor with 30 wt% GO was tested, in which it was exposed to the humidity firstly at 11% RH then at 58% RH, 75% RH and 85% RH successively for four times, respectively. At 11% RH, the sensor was exposed for about 150 s each time. Besides, a longer test time to 500 s was performed at the 58% RH, 75% RH and 85% RH for ensuring that the sensor can attain to the steady state.

Humidity hysteresis of the sensor was evaluated in the stage of absorption and desorption. The sensor was exposed firstly from 11% RH to 97% RH, and then from 97% RH back to 11% RH, continuously. Capacitance value was recorded when the sensor achieved the steady state at each relative humidity.

Characterization analysis

The appearance of NFC/GO/PDMS aerogel was photographed with digital camera to evaluate its appearance. Scanning electron microscope (SEM; S-3400N type; Hitachi, Japan) was employed to observe morphology of GO, NFC and NFC/GO/PDMS aerogel. Fourier transform infrared spectrometer (FT-IR; Nicolet iS50; Thermo Fisher Scientific, Inc., USA) was used to analyze GO, NFC and NFC/GO/PDMS aerogel, recording the corresponding spectrum in the wave number range of 400–4000 cm^{-1}. And the XPS spectrum of the aerogel was recorded by using X-ray photoelectron spectroscopy (XPS; ESCALAB 250XI+, Thermo Fisher Scientific, Inc., USA). It was noted that the aerogel was opened for 24 h in the same environment (25 °C, 60 ± 3% RH) before the test.

Density and porosity test

The density of the aerogel is closely related to its pore structure and specific surface area. Their density was calculated *via*

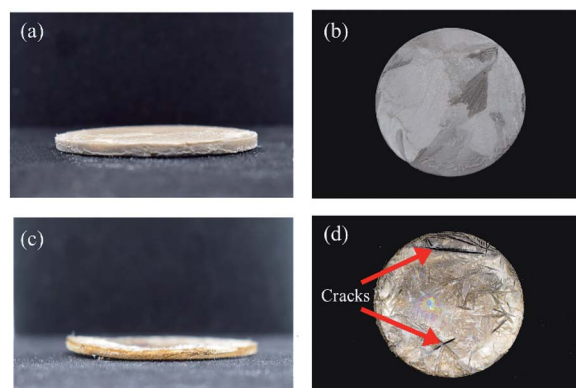Fig. 2 The diagram of humidity testing apparatus.

Fig. 3 Appearance of NFC/GO/PDMS aerogel in disk shape (a and b) added with anhydrous ethanol and (c and d) without anhydrous ethanol.

dividing their mass by volume. The porosity of NFC/GO/PDMS aerogel was estimated according to eqn (1):

$$\text{Porosity} = 1 - \frac{\rho}{\rho_c} \qquad (1)$$

where ρ was the density of the aerogel and ρ_c was the density of the solid material. Generally, the density (ρ_c) of NFC, GO and PDMS was about 1500 kg m^{-3}, 2100 kg m^{-3}, and 1040 kg m^{-3}, respectively.

Flexibility test

The compression test was carried out to explore the flexibility of NFC/GO/PDMS aerogel. The height of the aerogel with cylinder shape was firstly pressed down by 50% with binder plate, and then the binder plate was immediately picked up. After 1 min, its recovery process and recovery state were observed and evaluated.

Result and discussion

Morphology analysis

It is easy to form ice crystals in the process of vacuum freeze drying,[35,36] so cracks and gaps frequently appear in the NFC/GO/PDMS aerogel, which can reduce the uniformity and consistency of the three-dimensional porous network structure. It is not conducive to the absorption of water molecules. The addition of moderate anhydrous ethanol can prevent the generation of big cracks and gaps, which had been indicated in the existing research on rGO/carbon nanotube (CNT) sponge foam.[34] As seen in Fig. 3a and b, the aerogel with anhydrous ethanol exhibited smooth surface in which the porous network structure was well distributed, while there were many big cracks and gaps on the surface of the aerogel without anhydrous ethanol (Fig. 3c and d). The overall structure was relatively loose, as well as the structure uniformity of three-dimensional porous network was poor. Compared with other materials prepared by vacuum freeze drying technology,[37,38] the aerogel obtained a smoother and more complete surface which can promote conduction of water molecular and thus will improve humidity sensitivity.[39] Besides, the orderly morphology and structure also can be seen in the cylinder samples shown from Fig. 4.

As shown from Fig. 5, a big lamellar structure was formed in the GO aerogel (Fig. 5b) by the aggregation of thin and plicated sheets.[23] The obvious porous structure existed in the NFC aerogel along with much more flake pore wall shown in Fig. 5a. The
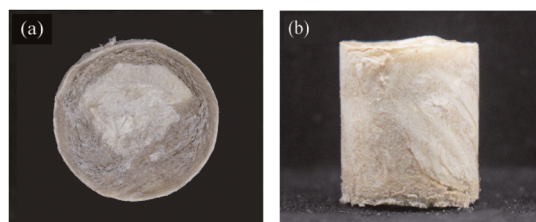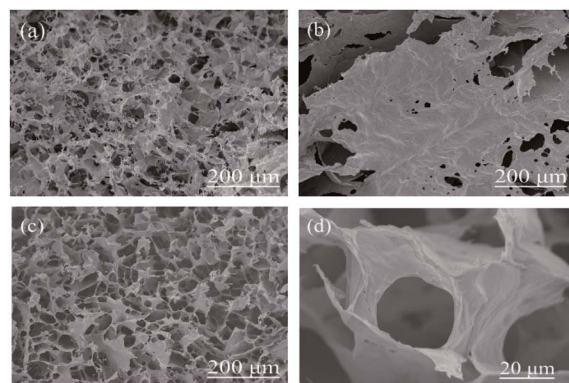

Fig. 5 SEM analysis of (a) NFC, (b) GO, and (c and d) NFC/GO/PDMS aerogel with 30 wt% GO.

NFC/GO/PDMS aerogel with 30 wt% GO (Fig. 5c) exhibited more orderly and uniform porous structure, in which NFC and GO cross-linked with each other. The structure would obtain accessible surface area and attract more water molecules.[40] In addition, Fig. 5d shows clear pore structure, which has sheet wall extending along the length of the oriented pore canal. This kind of porous network structure provides excellent ion diffusion channels and large active contact area,[41] which is of great significance to improve response sensitivity of the humidity sensor.

Chemical characterization analysis

Fig. 6a shows the FT-IR spectrum of the GO, NFC and NFC/GO/PDMS aerogel with 30 wt% GO. A strong absorption peak around the 3449 cm^{-1} was observed in the GO spectrum due to the stretching vibration of –OH group. In addition, the other characteristic peaks of GO appeared at 1637 cm^{-1}, 1386 cm^{-1} and 615 cm^{-1}, respectively, corresponding to C=C, C–OH and C=O groups.[18,23] For the pure NFC, the absorption peaks at 3449 cm^{-1}, 2928 cm^{-1}, 1633 cm^{-1}, 1426 cm^{-1}, 1028 cm^{-1} and
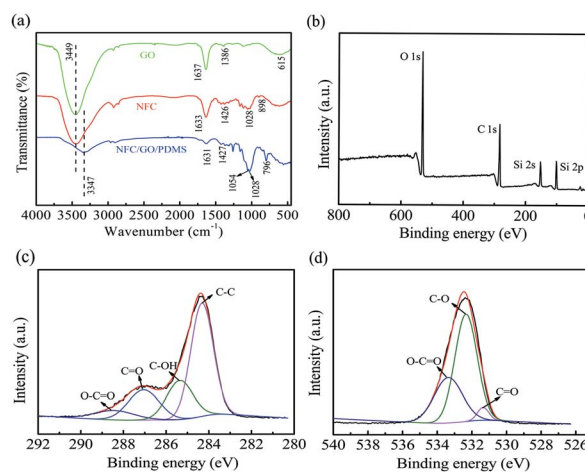

Fig. 6 (a) FT-IR spectra of GO, NFC, NFC/GO/PDMS aerogel with 30 wt%; XPS spectra of NFC/GO/PDMS aerogel with 30 wt% GO: (b) survey spectrum, (c) C 1s spectrum and (d) O 1s spectrum.

Fig. 4 Appearance on (a) top surface and (b) side face of NFC/GO/PDMS aerogel in cylinder shape added with anhydrous ethanol.

Table 1 Relative content of carbon and oxygen element in NFC/GO/PDMS aerogel with 30 wt% GO tested by XPS

Element	Content (at%)
Carbon	59.61
Oxygen	40.39

Fig. 7 The process of flexibility test on the cylinder sample: (a) original state, (b) the state when it was pressed down by 50% of the height, (c) the state when the pressure was released, (d) the state when the pressure was released after 1 min.

898 cm^{-1} are attributed to –OH stretching vibration, –CH stretching vibration, H–O–H stretching vibration, –CH$_2$ bending vibration, C–O–C stretching and C$_1$–H deformation vibrations, respectively.[42,43] According to the spectrum of NFC/GO/PDMS, there are also characteristic absorption peaks of the pure GO and NFC. However, the absorption peak of the –OH group shift to the lower wavenumber of 3347 cm^{-1} compared to that at 3449 cm^{-1} of pure NFC and GO, indicating the formation of strong hydrogen bonding in the aerogel.[44–49] After the addition of a small amount of PDMS, there is another strong absorption peak of Si–O–Si at 1054 cm^{-1}, and the absorption peak at 796 cm^{-1} is assigned to the action of Si–C groups.[50,51] In summary, the aerogel contains some oxygen-containing groups such as C–OH, C=O, H–O–H, C–O–C and Si–O–Si, which can effectively improve its adsorption effect to water molecules.[52–54]
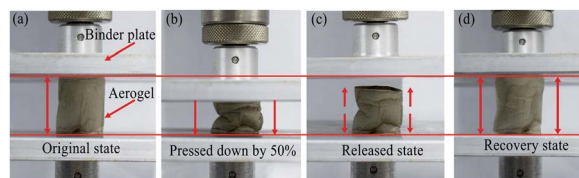
Similar results are also found from XPS analysis in Fig. 6b–d. It can be clearly seen that C and O are the main elements of the NFC/GO/PDMS aerogel with 30 wt% GO (Table 1). At the same time, there is also a small amount of Si element due to the addition of PDMS to enhance mechanical properties and adhesion force of the aerogel. Moreover, the C 1s spectrum is shown in Fig. 6c. The four types of carbon with different chemical states located at 284.3 eV, 286.4 eV, 287.1 eV and 288.6 eV, corresponding to C–C, C–OH, C=O and O–C=O groups, respectively.[25] As well as in Fig. 6d, three strong peaks can be observed in the O 1s spectrum, located at 531.2 eV, 532.3 eV and 533.4 eV, respectively, which are related to C=O, C–O and O–C=O groups.[31] The aerogel has similar groups to other existed GO composite humidity sensitive material, which had been proved that it has certain humidity sensitive characteristics.[24,25]

Density and flexibility analysis

It is found from Table 2 that the density of NFC/GO/PDMS aerogel is as small as 5.23 kg m^{-3}, which indicates that the aerogel has high porosity and specific surface area. The porosity of the aerogel is about 99.6% based on eqn (1). In general, the results demonstrated that the aerogel has low density and

porous structure, providing a large amount of open channels (SEM results in Fig. 5c and d). This structure increases the interaction surface area and facilitates the entry and exit of water molecules to enhance the sensitivity of sensor.[55]

It is found from Fig. 7 that the NFC/GO/PDMS aerogel has good flexibility through the elastic test on the cylinder sample. After the height of the aerogel was pressed down by 50%, it shrunk significantly at cylindrical surface. When the pressure was released, the aerogel almost entirely returned to its original appearance, and the height was basically the same to that before the compression. The found flexibility indicates its flexible skeleton and pore channel for sensing, by which its porous network structure can keep stable even that water molecules
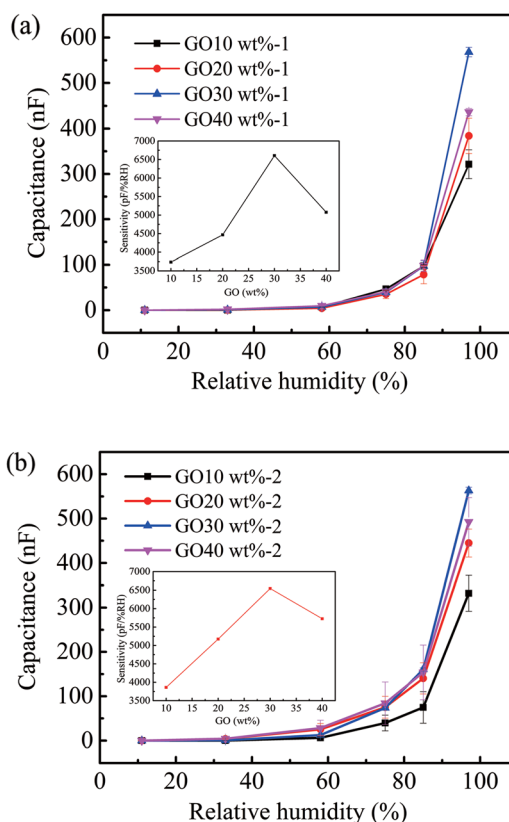
Fig. 8 (a and b) Relationship between capacitance and relative humidity of the twice-repeated sensors with different GO contents. The embedded figure displays the relation between the sensitivity and GO content.

Table 2 The density of the NFC/GO/PDMS aerogel

	Sample 1#	Sample 2#	Average value
Quality (g)	0.0546	0.0529	0.0538
Volume (cm^3)	9.90	10.67	10.29
Density (kg m^{-3})	5.52	4.96	5.23

eroded in its inner structure when stated in a high humidity atmosphere. The good flexibility as well as the stability could endow the sensor more suitable for actual detection,[56] and make it have more advantages in the application of wearable devices and flexible electronic instruments.

Humidity sensing performance

The NFC/GO/PDMS humidity sensor can absorb and desorb water molecules rapidly with the changing of the environment humidity, resulting in the change of the output capacitance. Fig. 8a and b shows that output capacitance of the sensor increased with the increase of relative humidity in the range of 11–97% RH, which exhibited a certain of regularity. Specifically, output capacitance of the sensor with 30 wt% GO increased from 11.71 pF to 565 583.33 pF in the humidity range of 11% RH to 97% RH.

Appropriate amount of GO promotes the humidity sensitivity of the sensor.[31] The sensitivity of sensor increased with raising the content of GO from 10 wt% to 30 wt%. The addition of 30 wt% GO gained a higher capacitance output value and sensitivity. As seen the microstructure of the aerogel with 30 wt% GO from Fig. 5c and d, GO and NFC cross-link to form a neat and orderly three-dimensional porous structure, which is conducive to the permeation of water molecules. Thus, the sensor can acquire capacitance change signals timely. However, excessive GO could result in that agglomeration and restack occurred on the surface of the aerogel (Fig. 5b), by which the effective surface area was reduced,[57] thus decreased the capacitance output value and the sensitivity of the sensor. Notably, the aerogel sample became shapeless and vulnerable as adopting the content from 50 wt% to 90 wt% of GO. When the content of NFC was gradually reduced, acting as binder and substrate, the structure of aerogel was weakened. Specifically, sensitivity of the sensor with 30 wt% GO was calculated as high as 6576.41 pF/% RH, while the reported capacitance sensors had sensitivity of −9.5 fF/% RH,[58] 46.25 pF/% RH,[59] 1061.6 pF/% RH,[60] 1552.3 pF/% RH,[61] 1604.89 pF/% RH,[62] and 1670.3 pF/% RH.[63]
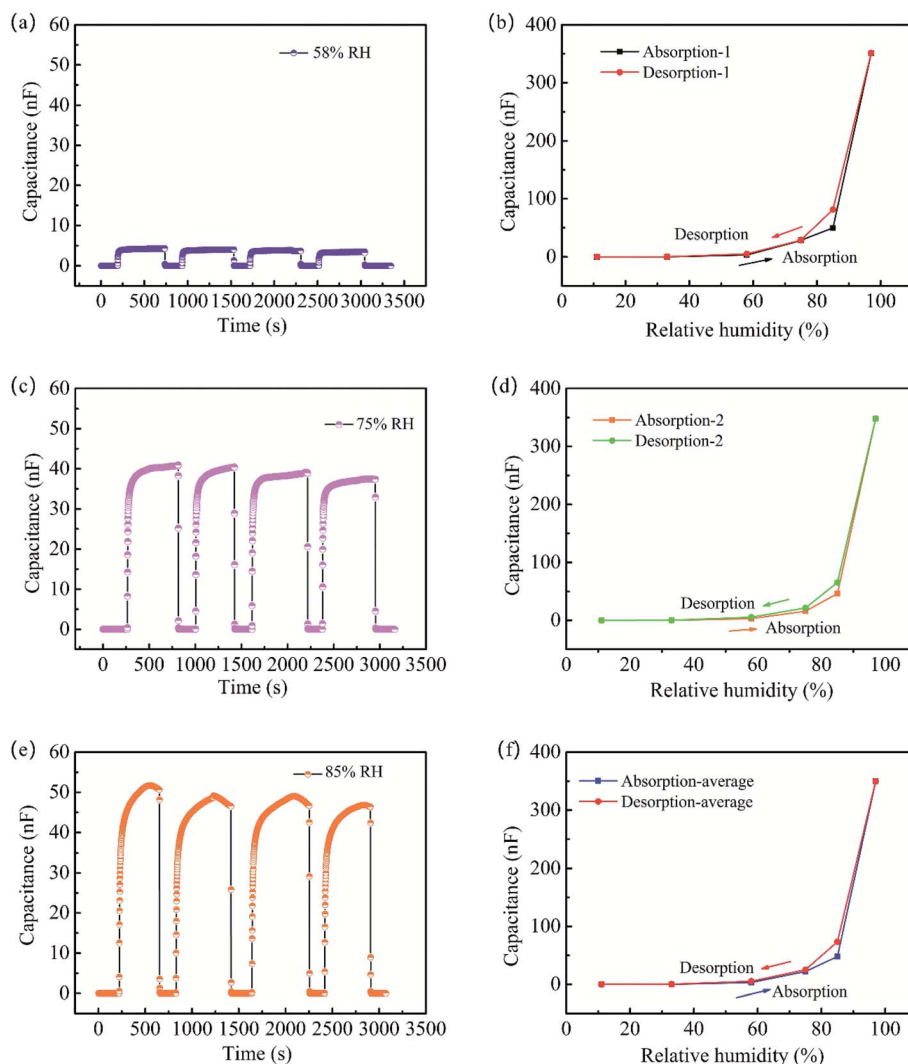

Fig. 9 The reproducibility of NFC/GO/PDMS humidity sensor with 30 wt% GO at (a) 58% RH, (c) 75% RH and (e) 85% RH; (b and d) humidity hysteresis curve of the two same sensors with 30 wt% GO, (f) humidity hysteresis curve based on the average test results of the two same sensors.

Fig. 9a, c and e indicates the excellent reproducibility of NFC/GO/PDMS humidity sensor. The stable output capacitance of the sensor with 30 wt% GO was demonstrated even it was exposed to various humidity for four times. It also can be seen in Fig. 9a, c and e that the output capacitance of the sensor was up to 4286 pF (58% RH), 38 113 pF (75% RH), and 49 108 pF (85% RH), correspondingly. The good reproducibility of the sensor makes it possible to provide stable humidity detection in practical applications.

Humidity hysteresis is an important performance index for humidity sensor.[64] Fig. 9b, d and f shows the humidity hysteresis curve of NFC/GO/PDMS humidity sensor with 30 wt% GO in the humidity range of 11–97% RH, reflecting that the sensor had a low hysteresis characteristic. Desorption curve of the sensor was slightly lagged behind its adsorption curve in the range of 75–85% RH. In the adsorption process, water molecules were firstly adsorbed on surface of the aerogel sensitive layer *via* the interaction with carboxyl, hydroxyl and other hydrophilic groups.[65] But the adsorbed water molecules are difficult to release for the effect of hydrogen bonding in the dehumidification stage, so the water molecules are partly remained in the inner structure of NFC/GO/PDMS aerogel,[66] resulting in desorption lag. It also can be seen from the Fig. 9b, d and f that the maximum humidity hysteresis occurred in the humidity of 85% RH.

Response/recovery time reflects the speed of dynamic output response of humidity sensor.[64] Fig. 10a and b shows the response/recovery time curve of the sensor with 30 wt% GO between the test humidity of 11% RH and 97% RH, in which the response time was 57 s and the recovery time was 2 s even the test were repeated multiple times. The recovery speed of this sensor was faster than other existed sensors.[59,60,62]

In addition, the performance of some reported sensors are also listed specifically in Table 3 for the comparison. Response time of the presented sensor was slightly longer, which need to be further improved in the future. The appearance of the humidity sensor with high sensitivity can be clearly seen in Fig. 10c.

Exponential growth relationship between the capacitance and relative humidity was found *via* fitting analysis shown in Fig. 11a. The fitted relationship of NFC/GO/PDMS humidity sensor-1 and NFC/GO/PDMS humidity sensor-2 were described as that $\lg y_1 = 0.05062x + 0.82714$ and $\lg y_2 = 0.05385x + 0.72361$ (y is the capacitance, pF; x is the relative humidity, % RH). Therefore, the humidity value corresponding to different electric capacity values can be calculated *via* the fitting equation. As shown in Fig. 11b, both the NFC/GO/PDMS humidity sensor and commercial hygrometer were put in an indoor environment (temperature 25.3 °C) to test its humidity at the same time, to evaluate practical performance of the sensor. After tested for 5 min, LCR digital bridge recorded the capacitance value (y) of 3880 pF under the stable state of the sensor. By calculating on basis of the above two fitted equations, the indoor humidity (x) indirectly measured by the presented sensor are 54.6% RH and 53.2% RH; it is 58.1% RH when it is directly tested using the commercial hygrometer. There is little relative deviation between the two test methods, indicating the practical application potential of the presented sensor.

The adsorption of water molecules and oxygenated groups are closely related to the response performance of humidity sensor.[67] Fig. 12 shows the humidity sensing mechanism of the NFC/GO/PDMS humidity sensor. As the sensor was stimulated by the external humidity, the NFC/GO/PDMS aerogel can physically adsorb water molecules, which will induce the change of
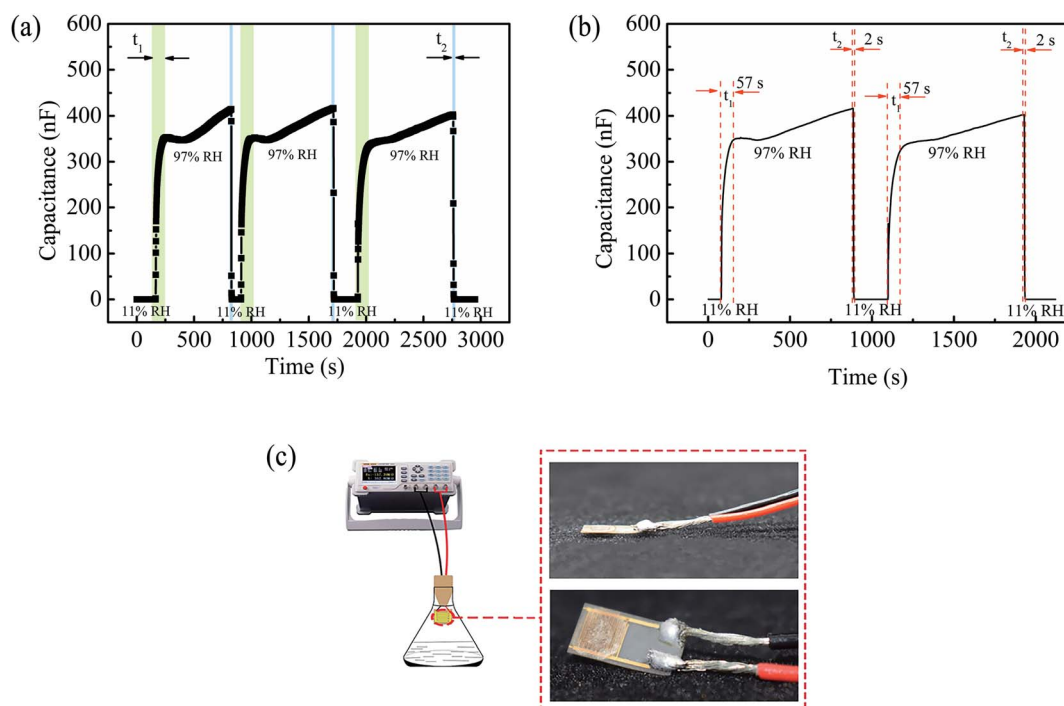

Fig. 10 (a and b) Response/recovery time curve of the sensor with 30 wt% GO in the test humidity at 11% RH and then 97% RH, continuously; (c) the measurement of sensing performance and the real state of the NFC/GO/PDMS humidity sensor.

Table 3 Comparison of the performance of different humidity sensors

| No.	Sensing material	Dry method	The test humidity range	Sensitivity	Response/recovery time	Ref.
1	GO	Baked for 2 h in the baking oven at 50 °C	25–65% RH	−9.5 fF/% RH	5 s/no mention of recovery time	58
2	GO	Dried in an air oven	15–95% RH	46.25 pF/% RH	10.5 s/41 s	59
3	GO/In_2O_3	Vacuum drying in an oven	11–97% RH	1061.6 pF/% RH	15 s/2.5 s	60
4	GO/PDDA	Dried in the oven at 50 °C for 2 h	11–97% RH	1552.3 pF/% RH		61
5	RGO/SnO_2	Vacuum drying in an oven	11–97% RH	1604.89 pF/% RH	102 s/6 s	62
6	GO/PPy	Dried naturally	11–97% RH	1670.3 pF/% RH		63
7	NFC/GO/PDMS	Vacuum freeze drying	11–97% RH	6576.41 pF/% RH	57 s/2 s	Our work
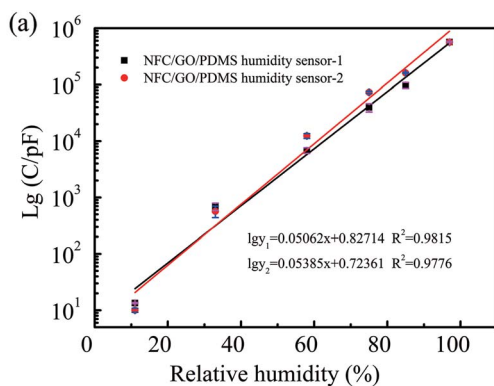
Fig. 11 (a) Fitting results of humidity sensitive characteristic curve of two same sensors with 30 wt% GO; (b) comparison between the test result of the NFC/GO/PDMS humidity sensor and commercial hygrometer.

Fig. 12 Humidity sensing mechanism for the NFC/GO/PDMS humidity sensor.

its dielectric constant and corresponding increase of capacitance, thus make the humidity sensor respond quickly.[68] It is observed from the SEM morphology that the NFC/GO/PDMS aerogel has an interconnected macroporous structure, forming a wide range of transmission channels with abundant reactive sites, which could promote the adsorption of water molecules and cause frequent protons hopping transport, so the humidity sensing performance can be enhanced.[68]

FT-IR and XPS spectra in Fig. 6 show that NFC/GO/PDMS aerogel contains a large amount of oxygen-containing functional groups, which play an important role in humidity sensing.[69] Simultaneously, the defects of GO also increase its interlayer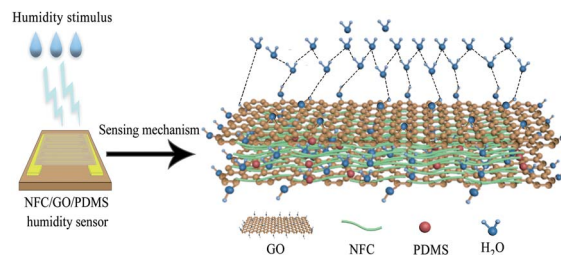 spacing, which helps the penetration of water molecules into internal interlayer space, ultimately improving the sensitivity of the humidity sensor.[70,71]

In the specific process of humidity sensing, water molecules are firstly adsorbed on the surface active sites of the aerogel through double hydrogen bonding.[72,73] With the increase of relative humidity, more and more water molecules are adsorbed through single hydrogen bonding.[73] The output capacitance of the humidity sensor increases gradually along with increasing the adsorption of water molecules.[73] This mechanism is also appropriate to this sensor.

In summary, the sensing characteristic of the NFC/GO/PDMS humidity sensor depends on the absorption of water molecules by the porous structure with oxygen-containing functional groups on its surface.

Conclusion

In this paper, a simple and environment-friendly technology was employed to fabricate a high-sensitivity, fast-response, rapid-recovery and flexibility humidity sensor. The NFC/GO/PDMS humidity sensor has high sensitivity (6576.41 pF/% RH) and low humidity hysteresis, and presents a fast response (57 s) and recovery (2 s) behavior. In which, NFC and GO construct a uniform three-dimensional porous network structure; the addition of PDMS enhances its stability and reproducibility; the addition of anhydrous ethanol in its preparation process can effectively inhibit the generation of ice crystal to obtain a homogeneous aerogel sensing layer.

There are a lot of hydrophilic groups on the surface of NFC/GO/PDMS aerogel constructed with the one and two-dimensional oxygen-containing monomer. Moreover, the

three-dimensional porous network structure of the aerogel provided a great deal of conduction channels and absorption active sites for water molecular, which enabled water molecules to penetrate freely, thus greatly improving the sensitivity of the sensor. The presented NFC/GO/PDMS humidity sensor finally realizes stable, reproducible and fast humidity sensing.

Conflicts of interest

The authors declare no conflict of interest.

Acknowledgements

References

1 T. H. Huang, J. C. Chou, T. P. Sun and S. K. Hsiung, *Sens. Actuators, B*, 2008, **134**, 206–212.

2 J. F. Feng, X. X. Kang, Q. Y. Zuo, C. Yuan, W. J. Wang, Y. H. Zhao, L. M. Zhu, H. W. Lu and J. Y. Chen, *Sensors*, 2016, **16**, 314.

3 H. Jin, X. Tao, B. Feng, L. Y. Yu, D. M. Wang, S. R. Dong and J. K. Luo, *Vacuum*, 2017, **140**, 101–105.

4 P. H. Zhu, Y. Liu, Z. Q. Fang, Y. D. Kuang, Y. Z. Zhang, C. X. Peng and G. Chen, *Langmuir*, 2019, **35**, 4834–4842.

5 U. Mogera, A. A. Sagade, S. J. George and G. U. Kulkarni, *Sci. Rep.*, 2014, **4**, 4103.

6 P. Jayaraman, C. Sengottaiyan and K. Krishnan, *J. Nanosci. Nanotechnol.*, 2020, **20**, 2893–2901.

7 N. Li, X. D. Chen, X. P. Chen, X. Ding and X. Y. Li, *IEEE Electron Device Lett.*, 2015, **36**, 615–617.

8 L. Y. Lan, X. H. Le, H. Y. Dong, J. Xie, Y. B. Ying and J. F. Ping, *Biosens. Bioelectron.*, 2020, **165**, 112360.

9 J. Majewski, *Metrol. Meas. Syst.*, 2017, **24**, 607–616.

10 H. Y. Zhang and S. J. Yang, *Advanced Graphic Communications and Media Technologies*, 2017, vol. 417, pp. 589–598.

11 Y. Feng, S. J. Gong, E. W. Du, K. Yu, J. Ren, Z. G. Wang and Z. Q. Zhu, *J. Mater. Chem. C*, 2019, **7**, 9284–9292.

12 H. Farahani, R. Wagiran and M. N. Hamidon, *Sensors*, 2014, **14**, 7881–7939.

13 X. Zhao, X. D. Chen, X. Yu, X. Ding, X. L. Yu and K. Tang, *Sens. Actuators, B*, 2019, **301**, 127048.

14 J. Boudaden, M. Steinmaßl, H. E. Endres, A. Drost, I. Eisele, C. Kutter and P. Müller-Buschbaum, *Sensors*, 2018, **18**, 1516.

15 C. Lv, C. Hu, J. H. Luo, S. Liu, Y. Qiao, Z. Zhang, J. F. Song, Y. Shi, J. G. Cai and A. Watanabe, *Nanomaterials*, 2019, **9**, 422.

16 D. Z. Zhang, J. Tong and B. K. Xia, *Sens. Actuators, B*, 2014, **197**, 66–72.

17 Y. Zhao, R. J. Tong, M. Q. Chen and F. Xia, *Sens. Actuators, B*, 2019, **284**, 96–102.

18 L. Chen, Z. Li, G. S. Wu, Y. D. Wang, T. Wang, Y. Ma and B. Fei, *Composites, Part A*, 2018, **115**, 341–347.

19 B. Liu, H. J. Sun, T. J. Peng, J. Z. Yang, Y. Z. Ren, J. Ma, G. P. Tang, L. L. Wang and S. K. Huang, *Appl. Surf. Sci.*, 2020, **503**, 144312.

20 Q. Fatima, A. A. Haidry, Z. J. Yao, Y. He, Z. Li, L. C. Sun and L. J. Xie, *Nanoscale Adv.*, 2019, **1**, 1319–1330.

21 W. P. Xuan, X. L. He, J. K. Chen, W. B. Wang, X. Z. Wang, Y. Xu, Z. Xu, Y. Q. Fu and J. K. Luo, *Nanoscale*, 2015, **7**, 7430–7436.

22 D. Z. Zhang, M. Y. Wang and Z. M. Yang, *Sens. Actuators, B*, 2019, **292**, 187–195.

23 D. Z. Zhang, X. Q. Zong and Z. L. Wu, *Sens. Actuators, B*, 2019, **287**, 398–407.

24 H. D. Peng, L. J. Meng, L. Y. Niu and Q. H. Lu, *J. Phys. Chem. C*, 2012, **116**, 16294–16299.

25 S. M. Xu, W. J. Yu, X. L. Yao, Q. Zhang and Q. Fu, *Compos. Sci. Technol.*, 2016, **131**, 67–76.

26 H. Golmohammadi, E. Morales-Narváez, T. Naghdi and A. Merkoçi, *Chem. Mater.*, 2017, **29**, 5426–5446.

27 K. Solin, M. Borghei, O. Sel, H. Orelma, L. S. Johansson, H. Perrot and O. J. Rojas, *ACS Appl. Mater. Interfaces*, 2020, **12**, 36437–36448.

28 P. H. Zhu, Y. D. Kuang, Y. Wei, F. Li, H. J. Ou, F. Jiang and G. Chen, *Chem. Eng. J.*, 2021, **404**, 127105.

29 Y. Yao, X. H. Huang, B. Y. Zhang, Z. Zhang, D. Hou and Z. K. Zhou, *Sens. Actuators, B*, 2020, **302**, 127192.

30 S. K. Mahadeva, S. Yun and J. Kim, *Sens. Actuators, A*, 2011, **165**, 194–199.

31 S. Pongampai, P. Pengpad, R. Meananeatra, W. Chaisriratanakul, A. Poyai, M. Horprathum, C. Chananonnawathorn, W. Titiroongruang and R. Muanghlua, *IEEJ Trans. Electr. Electron. Eng.*, 2020, **15**, 965–975.

32 A. Kafy, A. Akther, M. I. R. Shishir, H. C. Kim, Y. Yun and J. Kim, *Sens. Actuators, A*, 2016, **247**, 221–226.

33 J. K. Yuan, S. H. Yao, Z. M. Dang, A. Sylvestre, M. Genestoux and J. B. Bai, *J. Phys. Chem. C*, 2011, **115**, 5515–5521.

34 Y. R. Son and S. J. Park, *Chem. Eng. J.*, 2019, **373**, 1020–1029.

35 S. Facq, F. Danède and B. Chazallon, *J. Phys. Chem. A*, 2013, **117**, 4916–4927.

36 L. Xian, Y. Zhang, Y. J. Wu, X. Y. Zhang, X. Dong, J. C. Liu and A. R. Guo, *Ceram. Int.*, 2020, **46**, 1869–1875.

37 X. S. Ge, Y. N. Shan, L. Wu, X. D. Mu, H. Peng and Y. J. Jiang, *Carbohydr. Polym.*, 2018, **197**, 277–283.

38 S. M. Zhang, G. J. Liu, Y. Gao, Q. Y. Yue, B. Y. Gao, X. Xu, W. J. Kong, N. Li and W. Q. Jiang, *Sci. Total Environ.*, 2019, **694**, 133671.

39 Z. S. Xing, Y. Zheng, Z. F. Yan, Y. M. Feng, Y. Xiao, J. H. Yu, H. Y. Guan, Y. H. Luo, Z. Q. Wang, Y. C. Zhong and Z. Chen, *Sens. Actuators, B*, 2019, **281**, 953–959.

40 X. Y. Li, X. D. Chen, X. P. Chen, X. Ding and X. Zhao, *Mater. Chem. Phys.*, 2018, **207**, 135–140.

41 S. Y. Lyu, Y. P. Chen, L. F. Zhang, S. J. Han, Y. Lu, Y. Chen, N. Yang, Z. L. Chen and S. Q. Wang, *RSC Adv.*, 2019, **9**, 17824–17834.

42 C. Yang, C. C. Chen, Y. Y. Pan, S. Y. Li, F. Wang, J. Y. Li, N. N. Li, X. Y. Li, Y. Y. Zhang and D. G. Li, *Electrochim. Acta*, 2015, **182**, 264–271.

43 W. S. Chen, H. P. Yu and Y. X. Liu, *Carbohydr. Polym.*, 2011, **86**, 453–461.

44 X. P. Li, C. Shao, B. Zhuo, S. Yang, Z. Y. Zhu, C. W. Su and Q. P. Yuan, *Int. J. Biol. Macromol.*, 2019, **139**, 1103–1116.

45 Y. Y. Feng, X. Q. Zhang, Y. T. Shen, K. Yoshino and W. Feng, *Carbohydr. Polym.*, 2012, **87**, 644–649.

46 N. Song, X. S. Hou, L. Chen, S. Q. Cui, L. Y. Shi and P. Ding, *ACS Appl. Mater. Interfaces*, 2017, **9**, 17914–17922.

47 A. A. Ksenofontov, S. A. Stupikova, G. B. Guseva, E. V. Antina and A. I. Vyugin, *Sens. Actuators, B*, 2018, **277**, 462–466.

48 Y. Y. Sun, W. Fan, C. Zou, L. H. Wei, J. Q. Liu and Y. Xu, *ACS Sustainable Chem. Eng.*, 2019, **7**, 6851–6858.

49 Y. L. Gao and Z. X. Jin, *ACS Sustainable Chem. Eng.*, 2018, **6**, 6192–6202.

50 L. Wang, Y. Chen, L. W. Lin, H. Wang, X. W. Huang, H. G. Xue and J. F. Gao, *Chem. Eng. J.*, 2019, **362**, 89–98.

51 C. C. Chen, X. T. Bu, Q. Feng and D. G. Li, *Polymers*, 2018, **10**, 1000.

52 M. M. Mo, C. C. Chen, H. Gao, M. W. Chen and D. G. Li, *Electrochim. Acta*, 2018, **269**, 11–20.

53 K. L. Zhang, Z. L. Hou, B. X. Zhang and Q. L. Zhao, *Appl. Phys. Lett.*, 2017, **111**, 153101.

54 A. N. Parvez, M. H. Rahaman, H. C. Kim and K. K. Ahn, *Composites, Part B*, 2019, **174**, 106923.

55 J. Wu, Z. X. Wu, K. Tao, C. Liu, B. R. Yang, X. Xie and X. Lu, *J. Mater. Chem. B*, 2019, **7**, 2063–2073.

56 B. T. Li, G. Xiao, F. Liu, Y. Qiao, C. M. Li and Z. S. Lu, *J. Mater. Chem. C*, 2018, **6**, 4549–4554.

57 Y. L. Chen, Z. A. Hu, Y. Q. Chang, H. W. Wang, Z. Y. Zhang, Y. Y. Yang and H. Y. Wu, *J. Phys. Chem. C*, 2011, **115**, 2563–2571.

58 C. L. Zhao, M. Qin, W. H. Li and Q. A. Huang, *2011 16th International Solid-State Sensors, Actuators and Microsystems Conference*, Beijing, 2011.

59 H. C. Bi, K. B. Yin, X. Xie, J. Ji, S. Wan, L. T. Sun, M. Terrones and M. S. Dresselhaus, *Sci. Rep.*, 2013, **3**, 2714.

60 B. L. Li, Q. Tian, H. X. Su, X. W. Wang, T. E. Wang and D. Z. Zhang, *Sens. Actuators, B*, 2019, **299**, 126973.

61 D. Z. Zhang, J. Tong, B. K. Xia and Q. Z. Xue, *Sens. Actuators, B*, 2014, **203**, 263–270.

62 D. Z. Zhang, H. Y. Chang, P. Li, R. H. Liu and Q. Z. Xue, *Sens. Actuators, B*, 2016, **225**, 233–240.

63 M. Y. Wang, D. Z. Zhang, A. J. Yang, D. R. Wang and X. Q. Zong, *J. Mater. Sci.: Mater. Electron*, 2019, **30**, 4967–4976.

64 D. Z. Vasiljević, A. Mansouri, L. Anzi, R. Sordan and G. M. Stojanović, *IEEE Sens. J.*, 2018, **18**, 4378–4383.

65 V. V Perera, N. L. Fernando, B. Nissanka and D. R. Jayasundara, *Adsorption*, 2019, **25**, 1543–1552.

66 X. H. Le, X. Y. Wang, J. T. Pang, Y. J. Liu, B. Fang, Z. Xu, C. Gao, Y. Xu and J. Xie, *Sens. Actuators, B*, 2018, **255**, 2454–2461.

67 K. Rathi and K. Pal, *ACS Omega*, 2017, **2**, 842–851.

68 Z. Y. Wang, L. Y. Shi, F. Q. Wu, S. Yuan, Y. Zhao and M. H. Zhang, *Nanotechnology*, 2011, **22**, 275502.

69 H. L. Yan, S. Y. Guo, F. Wu, P. Yu, H. B. Liu, Y. L. Li and L. Q. Mao, *Angew. Chem., Int. Ed.*, 2018, **57**, 3922–3926.

70 V. I. Popov, D. V. Nikolaev, V. B. Timofeev, S. A. Smagulova and I. V. Antonova, *Nanotechnology*, 2017, **28**, 355501.

71 M. R. Karim, K. Hatakeyama, T. Matsui, H. Takehira, T. Taniguchi, M. Koinuma, Y. Matsumoto, T. Akutagawa, T. Nakamura, S. Noro, T. Yamada, H. Kitagawa and S. Hayami, *J. Am. Chem. Soc.*, 2013, **135**, 8097–8100.

72 B. Bhangare, S. Jagtap, N. Ramgir, R. Waichal, K. P. Muthe, S. K. Gupta, S. C. Gadkari, D. K. Aswal and S. Gosavi, *IEEE Sens. J.*, 2018, **18**, 9097–9104.

73 N. Li, X. D. Chen, X. P. Chen, X. Ding and X. Zhao, *RSC Adv.*, 2017, **7**, 45988–45996.